Advanced algorithms for early detection of first damage during static tensile tests

Davide D'Andrea, Danilo D'Andrea, Giacomo Risitano, Dario Santonocito
Department of Engineering, University of Messina, Contrada di Dio, Sant'Agata, 98166 Messina, Italy
davide.dandrea@studenti.unime.it, http://orcid.org/0009-0007-1555-4670
danilo.dandrea@unime.it, http://orcid.org/0000-0002-9809-8434
giacomo.risitano@unime.it, http://orcid.org/0000-0002-0506-8720
dariofrancesco.santonocito@unime.it, http://orcid.org/0000-0002-9709-9638

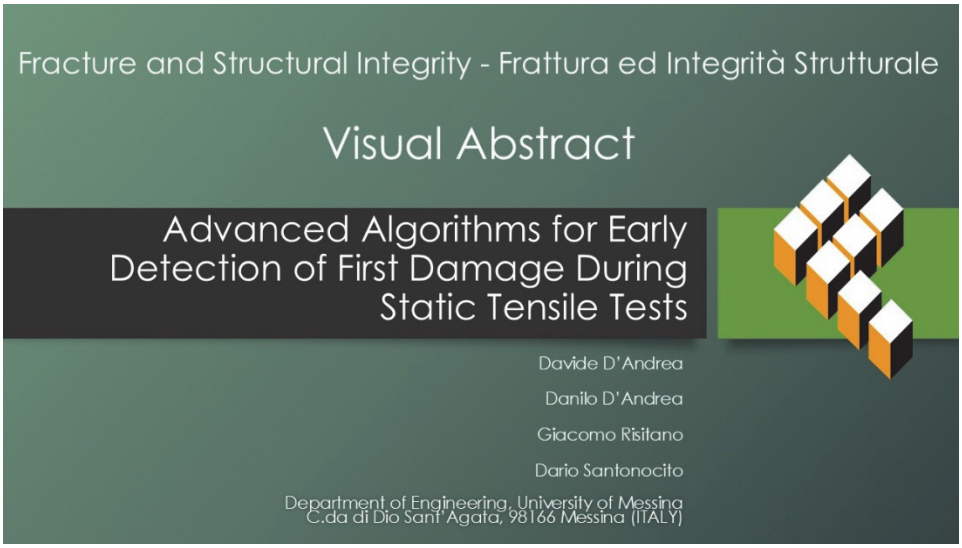

Citation: D'Andrea, D., D'Andrea, D., Risitano, G., Santonocito, D., Advanced algorithms for early detection of first damage during static tensile tests, Fracture and Structural Integrity, 74 (2025) 294-309.

Received: 09.06.2025
Accepted: 08.08.2025
Published: 08.09.2025
Issue: 10.2025

KEYWORDS. Fatigue, Thermography, Thermographic Method, Damage.

INTRODUCTION

Fatigue assessment of engineering materials remains a significant challenge for researchers worldwide, primarily due to the complexities involved in modelling this phenomenon. Factors such as material properties, environmental conditions, and different types of loads can drastically affect the ability of mechanical components to withstand time-dependent stress or strain. ASTM E466 and ASTM E606 standards require the S-N curve to be determined using five load levels, with each level applied to five specimens. The considerable expenditure of time, specimens, and money necessary for a detailed analysis of the material's fatigue properties often discourages designers from requesting information on the fatigue life of materials. In the modern industrial context, the mechanical characterization of materials, both from a static and fatigue perspective, needs to be conducted as quickly as possible while providing reliable results for design purposes. Thermographic Methods, through the analysis of energetic release of materials, offer insights into fatigue life in a short time with a limited number of specimens. These methodologies are now well-established and widely adopted by researchers globally, making them ready to transfer from academia to industry.
The Thermographic Method (TM), or Risitano's Thermographic Method (RTM), was first introduced by La Rosa and Risitano [1,2] and consisted in monitoring the surface temperature of specimens during fatigue tests by mean of infrared (IR) thermography as a full field contactless technique. RTM was applied on a large variety of materials such as steels [3,4],

welded joints [5,6], polymers [7] and composites [8,9]. The results obtained suggested that fatigue limit could be determined in less time than traditional methods with good accuracy.
In 2013, Risitano and Risitano [10] proposed the Static Thermographic Method (STM) as a technique to obtain in a rapid way a design parameter linked to fatigue limit by analysing energy release during a monotonic quasi-static tensile test. The advantages are enormous, as just one day of testing and a few samples are enough to obtain important information on the material damage process, which can be observed in the sample's surface temperature over time. This thermal trend presents three distinct phases, starting with a linear decrease in temperature, followed by a deviation from the initial linear trend in the second phase due to the onset of irreversible deformations, and finally, an exponential increase in temperature upon reaching the yield point.
Its main limitation is the difficulty of data's analysis, which needs understanding of the thermal behaviour of the materials under quasi-static tensile load and capability of correlate several information acquired by different devices at different sample frequencies. Since it was used for the first time, it was strictly dependent on the subjectivity of those analysing data, whose experience suggested how to define subsets to obtain limit stress, considering noise linked to measurement devices and material thermal behaviour, which is always different.
To make the prediction of STM the more objective as possible, not just relying on the operator's experience, and adoptable for users outside the research field, several methodologies have been implemented using Python language. The goal is to automatically assess the limit stress, i.e. the macroscopic stress level at which damage begin within the material and make the STM an useful and time-saving methodology for mechanical design. In [11], Colombo et al. analysed temperature's data derived from monotonic quasi-static tensile test performed on Ti-6Al-4V through an iterative algorithm whose aim is to define the thermoelastic trait of temperature's trend over time by increasing the number of points to the subset on which a linear regression is done until a determination coefficient higher than 0.985 is reached, while in [12] Crisafulli et al. used an iterative approach based on the definition of a bilinear model for temperature's data fitting. Both methods resulted to be effective to spot inflection point in temperature's trend over time but could be affected by signal quality and noise which characterize this kind of IR acquisition.
For this reason, a robust algorithm, specifically tailored to align with the assumptions and recommendations of the Static Thermographic Method (STM) theory was proposed. This approach was preferred over standard change-point detection techniques which may not fully account for the specific characteristics and constraints inherent in the STM framework.

THEORETICAL BACKGROUND

Risitano's Thermographic Method (RTM)

The RTM consists in determining the stabilization temperature associated to the stress level applied to the specimen. Surface temperature trend shows three different phases: the first phase in characterized by a temperature growth until a stabilization temperature is reached. Temperature remains constant throughout the second phase, since it reached its stabilization value ΔT_{st} and rises again in the third phase before the failure of the specimen. It is possible to determine the Energy Parameter Φ calculated as the area under the curve describing temperature's trend over number of cycles N (measured as cycles·K). It was observed that the higher the applied stress, the higher the stabilization temperature value will be, and that the Energy Parameter remains constant regardless of the applied stress, following the relation:

$$\Phi = N_i \Delta T_{st} \tag{1}$$

The fatigue limit is finally calculated as the stress level which correspond to a negligible increase in temperature ($\Delta T_{st} \sim 0$ *K*). RTM was largely used and improved by many researchers [13,14].

Static Thermographic Method (STM)

The thermal behaviour of a material under a quasi-static tensile load consists in three thermal phases (Fig. 1). In the first phase (Phase I) it is observed a linear cooling of the surface temperature according to the thermoelastic effect enunciated by Lord Kelvin:

$$\Delta T_s = -\frac{\alpha}{\varrho \cdot c} T_0 \cdot \sigma_1 = -K_m T_0 \cdot \sigma_1 \tag{2}$$

In Eqn. 2, ΔT_s stand for surface's temperature, α is the coefficient of thermal expansion, ϱ is the material density, σ_1 is the uniaxial applied stress, T_0 is the absolute temperature of material and c is its specific heat capacity at constant pressure; K_m is the thermoelastic constant.
In the second phase (Phase II) it can be observed a deviation from the initial linear trend, caused by appearance of the first microdamage, until a minimum value of temperature is reached at the yield stress of the material (σ_y). In the third phase (Phase III) there is an exponential growth of temperature until the failure of the material. In Eqn. 3, it is reported the mathematical model proposed by Melvin [15] which incorporates the positive contribution of dissipated plastic energy to characterize the surface temperature of a specimen during a static tensile test.

$$\Delta T=-K_m T_0 \sigma_1-\frac{B\sigma_1^2}{3cE} \tag{3}$$

Where B is the drag coefficient, linked to the Burges vector b and E is the Young's Modulus. It is composed of a first elastic component and a second plastic component, whose contribute to a positive temperature change due to damage, since the drag coefficient B is negative. The mathematical model proposed by Melvin is difficult to apply in practical applications due to the uncertainty in the assessment of the coefficients, so simpler models have been proposed.

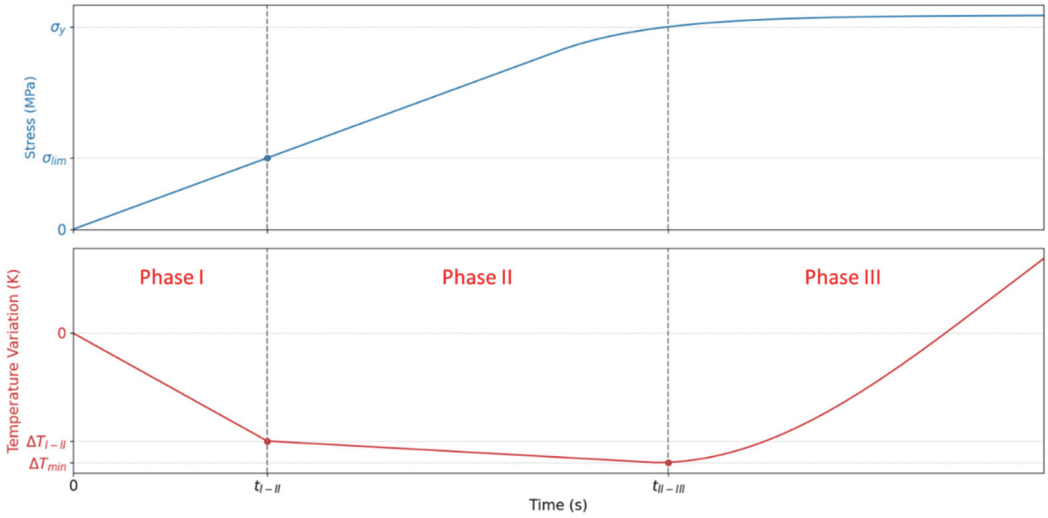

Figure 1: Schematic representation of thermal phases during a quasi-static tensile test.

In Fig. 1, stress and thermal trends over time measured during a static tensile are reported. The limit stress (σ_{lim}) can be estimated as the stress measured at the instant t_{I-II}, when the change in slope occurs between Phase I and Phase II at the temperature ΔT_{I-II}. The time value t_{II-III} is the instant delimiting Phase II and Phase III and it corresponds to the instant in which yield stress occurs. The deviation from linearity happens because of the presence of internal microdefects which growth when subjected to an increasing tensile force. Risitano and Risitano stated that the limit stress, occurring at the inflection point between Phase I and Phase II, can be seen as the stress level at which first micro damage arises. Since the change in slope depends on test velocity, material properties and manufacturing techniques, it is difficult to identify the subsets of thermal points of Phase I and Phase II. In previous works this was made according to the operator's experience; however, it is necessary to automate the procedure of identification of the limit stress.
For further details on RTM and STM the reader can refer to [1,2,10,12,16].

MATERIALS AND METHODS

Two different experimental setups were adopted in previous works of these authors, respectively, for plastic and metallic specimens to calibrate the algorithms developed in the present work.

Tensile tests on plastics were performed adopting the FFM (Fast Fatigue Machine), a pneumatic benchtop testing machine with a 2.5 kN load cell patented by the University of Messina's academic spin-off KnoWow S.r.l. and produced by ItalSigma S.r.l.. It is designed for the use of thermographic methods and is equipped with two easily adjustable mounts with a video camera (Basler camera acA2440-35uc, 35 fps, 2464 x 2056 at full resolution) for Digital Image Correlation (DIC) and an IR camera (Irtech model XT, thermal sensitivity 80 mK, detector UFPA 382 x 288 pixel @ 80 Hz/ 27 Hz). Experimental setup is represented in Fig. 2.

Figure 2: Fast Fatigue Machine with IRtech XT IR camera and Basler camera acA2440-35uc for DIC.

The plastic specimens were designed according to ASTM D638. The 2.5 kN load cell imposed to choose the type V specimen geometry with a thickness of 2 mm for Nylon-CF15 [17] produced by Fillamentum (PA12 filament reinforced with carbon fibres) and 3 mm for PA12 MultiJet Fusion [18]. Tests were performed in displacement control adopting a crosshead speed of 0.04 mm⁄s on both materials.
Stainless steel AISI 316L specimens were designed following ASTM E466 standards and were tested on a servo hydraulic 250kN MTS 810 machine in stress control with a stress rate of 6 MPa/s. IR thermal images were acquired with IRtech XT model, equipped in the Fast Fatigue Machine, and FLIR A40 infrared thermal camera for metallic specimens, whose thermal sensitivity is 80 mK for both cameras. Temperature data were extracted from Timage Connect software and Flir SDK toolkit and the algorithm for data processing was developed in Python language.

APPROACHES FOR THE IDENTIFICATION OF THE THERMAL PHASES

The aim of the STM is to identify the macroscopic stress level, applied monotonically during a quasi-static tensile test, at which the loss of linearity of the thermal decrement occurs. In previous works, thermal phases were identified manually by an expert operator who had to try to find the best combination of first and second phases to obtain analytically corresponding inflection point ($\Delta T_{I\text{-}II}$). To do this, the operator had also to choose the point at which Phase III start. To make the method more accessible to everyone, from an unexpert operator up to a skilled one, two strategies have been developed: the first is operator-assisted, while the second is based on an iterative method.

Operator-aided method for the identification of thermal phases

The first developed approach consists in interactively selecting on the temperature vs. time graph the points where the transition from Phase I, Phase II and Phase III approximately occur. In this way, it is easy for the operator to distinguish and divide thermal phases by pointing it manually. The subsets of temperature data obtained are used to perform a linear regression for Phase I and II. The resulting equations are then used to calculate the intersection point and to extract the corresponding stress value. It should be emphasized that it is up to the operator to verify the quality of the model. In Fig. 3, it can be observed the interactive subdivision of the thermal trends. Vertical red line corresponds to the point chosen by the operator as transition between Phase I and Phase II.

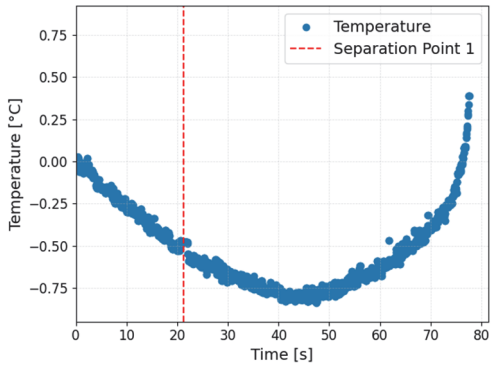

Figure 3: Interactive selection of subsets separator in thermal trend.

This approach freed operator from coding knowledge, but not from phenomena understanding; indeed, it is suitable for expert operator with a deep knowledge of the STM.

Iterative method: Bilinear model definition of the cooling process

The second approach has been implemented to make the method not operator dependent. Given the short length of data to be analysed, it has been chosen to operate in an iterative way. At first, temperature vs. time signal is filtered from outliers using interquartile range (IQR) method [19], which consists of equally splitting the dataset into four range named quartiles; the IQR is then used to distinguish outliers from useful data. A value is considered as an outlier if it falls outside a range defined by a threshold based on the IQR, typically set at 1.5 times the IQR above the third quartile or below the first quartile. In this way, the temperature dataset has been divided in two subsets a priori. The first dataset starts at a fixed time, expressed in percentage of test duration (to avoid possible temperature noise at the beginning of the test), and finishes in a variable moment, which is the varying parameter of the iterative process; the second subset start at the same instant at which the first one ends, and it finishes at the time in which the minimum temperature occurs. At the end of each iteration, the dividing point is translated forward of a temperature data point and it is used to identifies subsets. In Fig. 4 are represented three samples of iterative subset separation process at 20%, 50% and 80% of the iterative process. The three temperature phases are distinguished adopting three colours (blue for Phase I, red for Phase II and green for Phase III). As the iterative process go forward, the subset lengths of Phase I and Phase II are adjusted while Phase III remains fix.

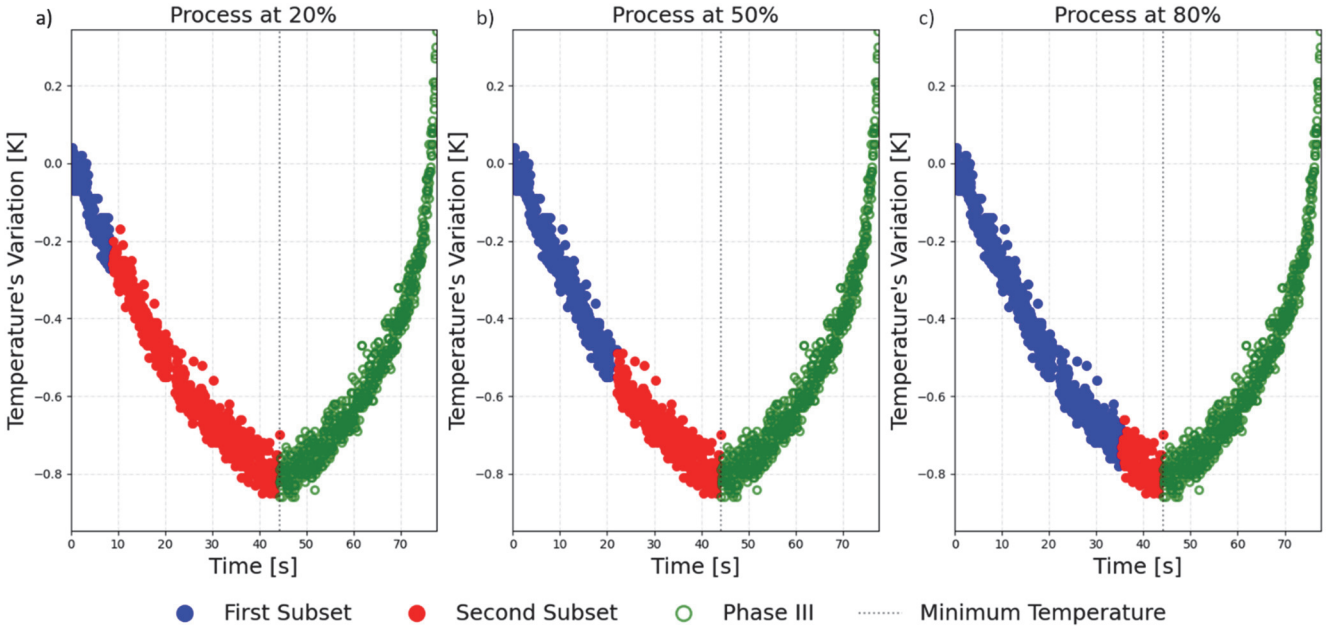

Figure 4: Phase I and II subsets separation at a) 20%, b) 50% and c) 80% of the iterative process.

The subsets for Phase I and II, constructed in this way, are then used to make linear regressions of temperature vs. time ($\Delta T = m\,t + q$) and estimate the linear regression coefficients m_1, m_2, q_1, q_2. These coefficients are than used to calculate the intersection between the linear regression of Phase I and Phase II, which is the point where the limit stress can be determined (Eqn. 4).

$$\begin{cases} t_{int_i} = \dfrac{q_2 - q_1}{m_1 - m_2} \\ \Delta T_{int_i} = m_1 t_{int\,i} + q_1 \end{cases} \tag{4}$$

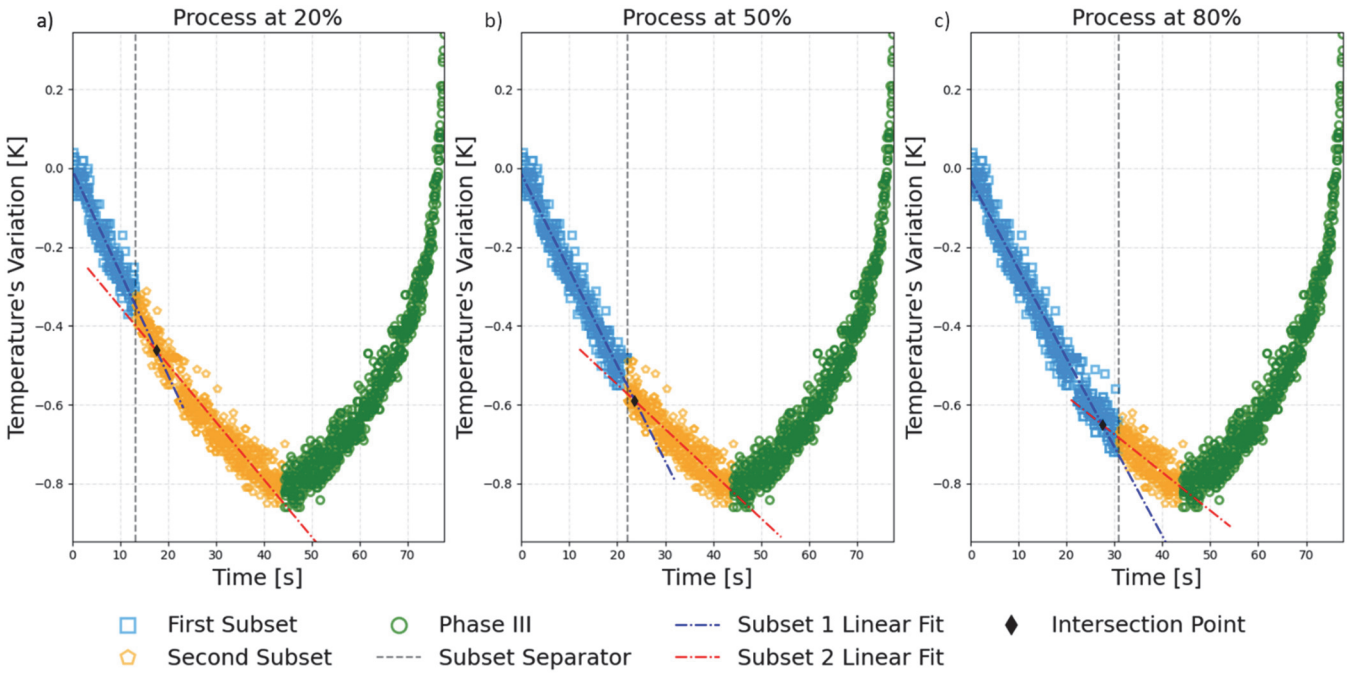

Figure 5: Linear regressions of subsets and intersection point calculations at: a) 20%, b) 50% and c) 80% of iterative process.

In Eqn. 4, $t_{int,i}$ and $\Delta T_{int,i}$ are, respectively, the instant and temperature at which intersection is located and calculated for each iteration. In Fig. 5, it is represented how the intersection points and the relative lines vary during the iterative process. The intersection point values are then used to determine the actual Phase I and Phase II (ΔT_I, ΔT_{II}), using the time corresponding to the intersection between the lines as a discriminant:

$$\begin{cases} \text{Phase I: } \Delta T_I(t) \text{ for } t \le t_{int\,i} \\ \text{Phase II: } \Delta T_{II}(t) \text{ for } t > t_{int\,i} \end{cases} \tag{5}$$

They are also used to create the bilinear model in each iteration ($\Delta T_{bl,i}$)describing the linear trends calculated before as a composite function defined as it follows:

$$\Delta T_{bl_i}(t) = \begin{cases} m_1 t + q_1, & t \le t_{int\,i} \\ m_2 t + q_2, & t > t_{int\,i} \end{cases} \tag{6}$$

Finally, the bilinear model is adopted to represent the cooling phenomenon during a quasi-static tensile test.
The algorithm calculates every possible combination of first and second subsets, and consequently every possible bilinear fitting model. The key advantage of this methodology lies in its ability to identify the point of slope change regardless of the material, making the algorithm material independent.

A flowchart describing every algorithm step is reported in Fig. 10. Each iteration is identified by the index i, and the process terminates when i reaches the last element in the array identified by the index "end", corresponding to the length of the array (i.e., the last valid index in the array). Process has been divided in two phases: The preprocessing phase consists in choosing parameters defining first attempt subsets and linear regressions calculation described in this section. The optimization parameters phase consists in calculating coefficients used to determine the most adequate bilinear model. The process repeat itself reducing threshold value for outliers' detection until limit stress values estimated by every method match.

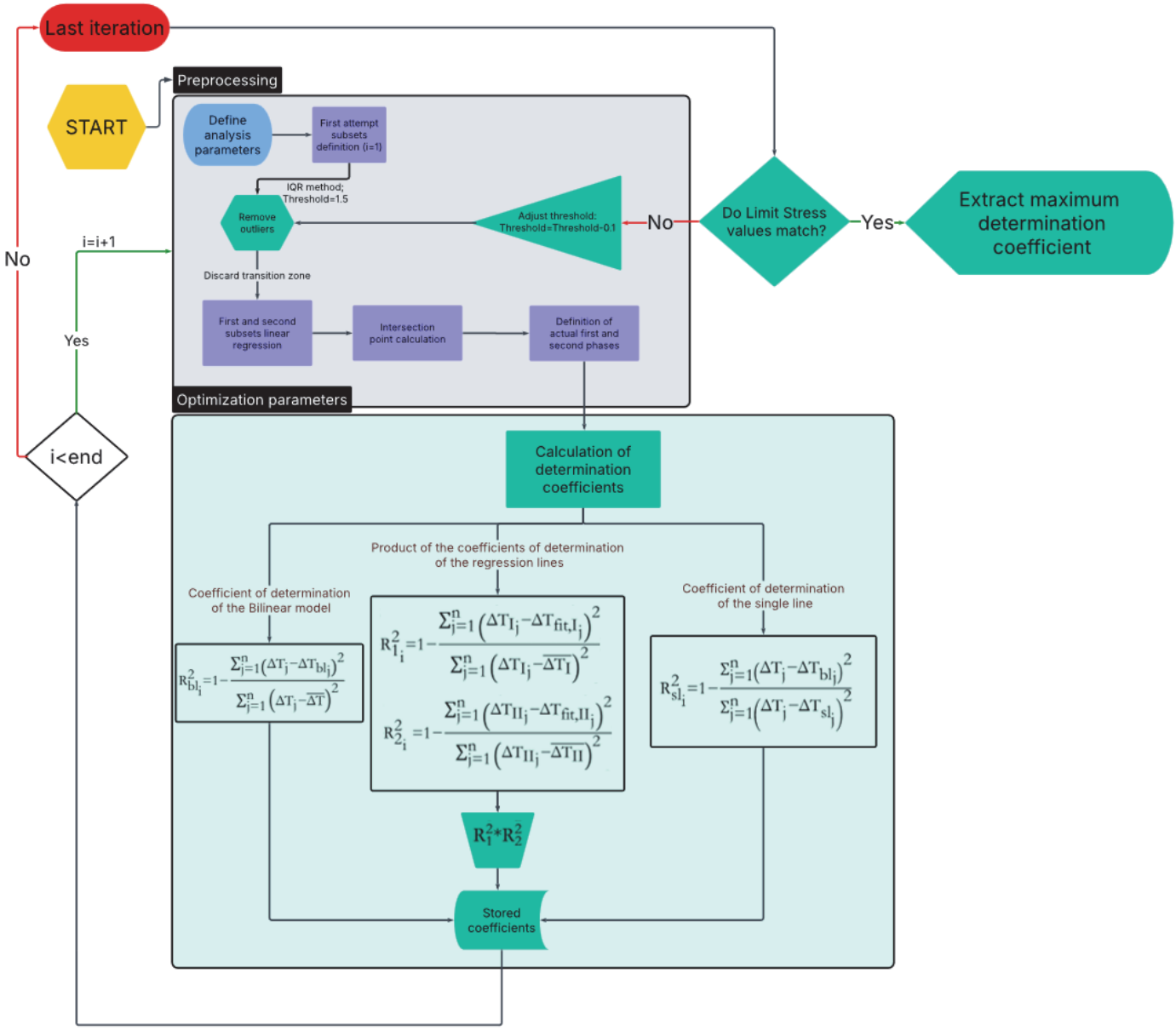

Figure 6: Algorithm flowchart.

Optimal parameters for the estimation of thermal phases with bilinear model

In the following section, three parameters have been discussed to find out which is the optimal combination of first and second subsets. The first parameter taken into account is the coefficient of determination of the bilinear model (R_{bl}^2); the second parameter is the product of the coefficient of determination of the first and second regression lines

($R^2_{1,i} \cdot R^2_{2,i}$); finally, the third parameter is a coefficient that indicates how well the bilinear model approximates the experimental data respect a single straight line. These parameters will be discussed in the following.

Coefficient of determination of the Bilinear model

The coefficient of determination for the bilinear model, R_{bl}^2, is estimated for each iteration and stored in the algorithm memory, allowing to extract its maximum value.

$$R^2_{bl_i} = 1 - \frac{\sum_{j=1}^{n} \left(\Delta T_j - \Delta T_{bl_j} \right)^2}{\sum_{j=1}^{n} \left(\Delta T_j - \overline{\Delta T} \right)^2} \tag{7}$$

In Eqn. 7, index i stands for the iteration and index j stands for the single experimental data point. The term ΔT represents raw data, ΔT_{bl} indicates the bilinear fitted model and $\overline{\Delta T}$ the mean value of experimental data.
Since it has been observed that noisier signal is located in the transition zone between Phase I and Phase II, the approach has been implemented to exclude the final portion of the first subset and the initial portion of the second subset from the linear regression calculations. By doing so, the linear trends are imposed by the less noisy temperature regions. In Fig. 7 it has been chosen to discard 10% of first subset in its end and 20% of second subset at the beginning. Additionally, raw data is cleaned of outliers using the interquartile range (IQR) method. Since it cannot be defined a fixed threshold a priori due to variability of data quality, which is linked to IR camera, room's conditions and random events, the sensitivity of this method is also subject to iterative analysis that adjusts the amount of data considered as noise.

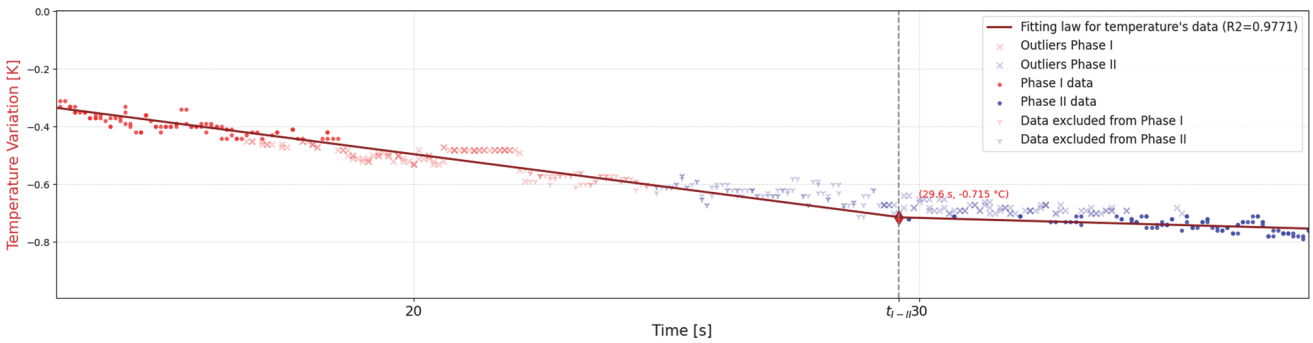

Figure 7: Temperature data between Phase I and Phase II excluded from calculation (shaded red and blue markers).

Product of the coefficients of determination of the regression lines

To demonstrate the validity of the iterative approach, two other ways to calculate the limit stress were implemented.
The first one consists of determining the best combinations of Phase I and Phase II, by calculating the coefficient of determination for both lines with respect to the actual thermal phases distinguished through the previously identified intersection point:

$$R^2_{1_i} = 1 - \frac{\sum_{j=1}^{n} \left(\Delta T_{I_j} - \Delta T_{fit,I_j} \right)^2}{\sum_{j=1}^{n} \left(\Delta T_{I_j} - \overline{\Delta T_I} \right)^2} \tag{8}$$

$$R^2_{2_i} = 1 - \frac{\sum_{j=1}^{n} \left(\Delta T_{II_j} - \Delta T_{fit,II_j} \right)^2}{\sum_{j=1}^{n} \left(\Delta T_{II_j} - \overline{\Delta T_{II}} \right)^2} \tag{9}$$

In Eqns. 8 and 9, ΔT_I and ΔT_{II} are the actual Phase I and Phase II, and $\Delta T_{fit,I}$ and $\Delta T_{fit,II}$ are the values obtained from the fitting.

The product $R_1^2 * R_2^2$ is calculated, and the result of the iteration in which this product is maximized is chosen to represent the best combination of individual lines.

Coefficient of determination of the single line

Since the coefficient of determination can be interpreted as a parameter of how well the numerical model approximates the experimental data compared to what would happen using the mean value, it was decided to use the parameter R_{sl}^2 (single line) which indicates how well the bilinear model approximates the experimental data compared to a single line. Its formula is reported in Eqn. 10. Representation of this comparison is reported in Fig. 8 where, as the iteration go forward, the bilinear model is optimized.

$$R_{sl_i}^2 = 1 - \frac{\sum_{j=1}^{n} \left(\Delta T_j - \Delta T_{blj} \right)^2}{\sum_{j=1}^{n} \left(\Delta T_j - \Delta T_{sl_j} \right)^2} \tag{10}$$

In Eqn. 10, the index i stands for iterations, while the index j stands for instantaneous data points. ΔT is the experimental data, ΔT_{bl} is the temperature value obtained by bilinear model and ΔT_{sl} is the temperature value calculated by fitting experimental data with a single straight line. Even in this case, coefficients deriving from each iteration are stored and the bilinear model characterised by the highest value of R_{sl}^2 is extracted at the end of the process.

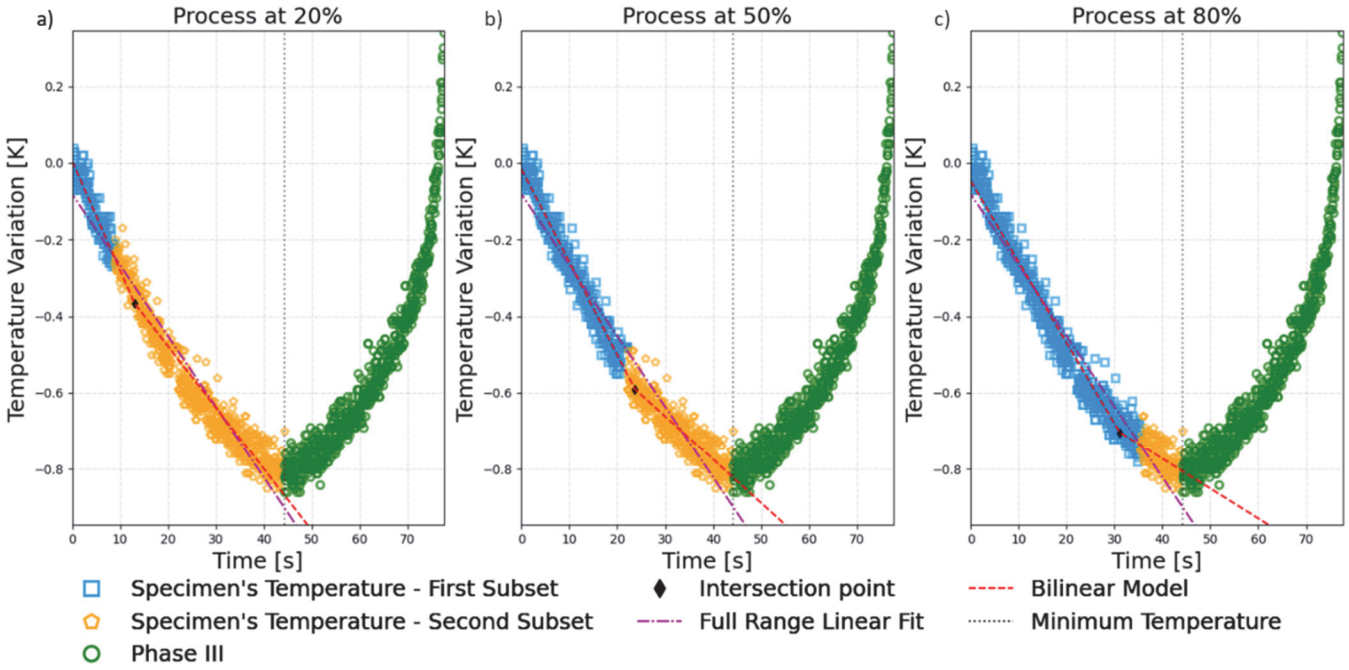

Figure 8: Comparison between bilinear model and single line fitting at a) 20, b) 50 and c) 80% of iterative process.

Generally, the optimization parameters previously considered lead to different values of the limit stress; however, after optimizing the threshold sensitivity of the interquartile range method, the limit stress values coincide. This process involves comparing the limit stress values obtained using the three methods described above. If these values do not match, the threshold (initially set to 1.5) is reduced and the data are reanalysed until convergence of results. The initial threshold's value of 1.5 is empirically motivated: it effectively identifies data points that are significantly distant from the median of the dataset while minimizing the risk of incorrectly flagging normal values as outliers. The stopping criterion is defined such that the iterative loop terminates when the IQR threshold reaches a value of 0. This corresponds to the extreme case in which all data points outside the interquartile range are discarded. In Fig. 9 it can be observed STM result obtained at the end of the optimizing process described. Stress levels resulting from maximizing, respectively, the coefficient of determination of the bilinear model, the product of the coefficient of the determination of the regression lines and the coefficient of

determination of the single line were compared and used as a target for interquartile range method's threshold adjustment. Each coefficient associated to the optimal model is reported in the legend.

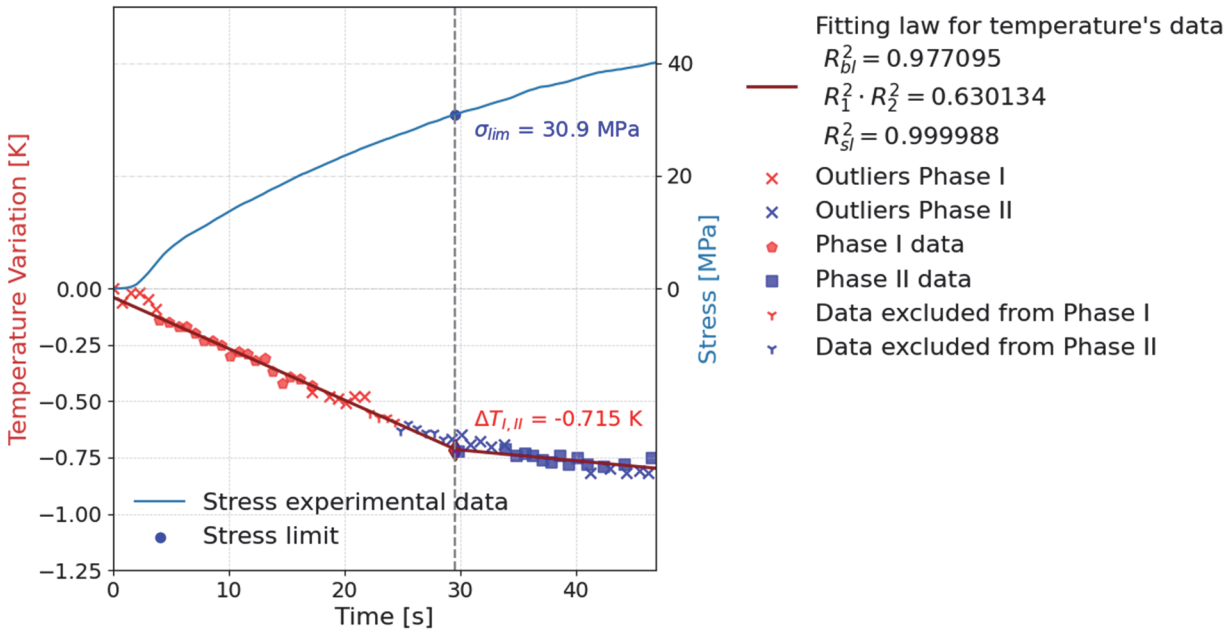

Figure 9: STM optimal result deriving from comparison between limit stress obtained by Bilinear Model, Regression of Individual Straight Lines and Regression with respect to complete line.

Validation of the proposed algorithm and comparison with Risitano's Thermographic Method

Results obtained with the algorithm described in previous section were compared with the ones obtained with RTM applied on the same materials. It was observed that results are in good agreement, confirming the reliability of the method [20]. Percentage differences between STM and RTM results defined as in Eqn. 11 are reported in Tab. 1 together with calculated stress limits.

$$E_{\%} = \left| \frac{\sigma_{lim,STM} - \sigma_{0,RTM}}{\sigma_{0,RTM}} \right| \cdot 100 \tag{11}$$

It has to be remarked how the bilinear model is a simplification of the thermal cooling phenomenon, since the heat generated during Phase II, linked to the onset of damage, may cause nonlinearities. More complex models have to be implemented to accurately describe the thermal trend; however, to assess the transition point between Phase I and II, linear regression can be adopted.

In Fig. 10 and 12 results for PA12 MJF are reported. Fig. 11 shows stress and thermal trend over time. It can be observed how the subsets used for calculation do not correspond to actual Phase I and Phase II, since they are determined by inflection point defined as the intersection between linear regressions. For this test it has been chosen to discard 10% of data in the end of first phase and 20% in the beginning of second phase, excluding transition zone from calculations. Stress limit is extracted from stress vs. time curve at the same time as the change in slope temperature's trend occurs.

Results of the STM obtained by graph visual inspection (Predicted) and those obtained by the described algorithm (Calculated) for PA12 MJF, Nylon CF15 and AISI316L are reported in Tab. 1, together with the number of observations (n), the Student's t value for a 95% confidence level with a two-tailed distribution (t^*), and the corresponding 95% confidence interval (CI) calculated with Eqn. 12, where $\overline{\sigma_{lim,STM}}$ is the average value of the stress limit and s is the standard deviation.

$$CI_{95\%} = \overline{\sigma_{\lim,STM}} \pm t^{*} \cdot \frac{s}{\sqrt{n}} \tag{12}$$

Material	σ_{lim} [MPa] STM - Predicted	σ_{lim} [MPa] STM - Calculated	Observations number - n	Student's t - t^{*}	$CI_{95\%}$ [MPa] - Calculated
Nylon CF	30.1	31.7	4	3.182	30.1 ± 2.0
	29.3	29.7			
	28.0	28.7			
	25.5	30.5			
PA12 (MJF)	27.2	31.4	3	4.303	30.3 ± 3.7
	27.8	28.6			
	28.0	30.9			
AISI 316L	201.0	204.5	3	4.303	219.4 ± 60.3
	212.0	247.4			
	200.0	206.3			

Table 1: STM experimental report.

Fig. 11 shows stabilization temperature vs. stress amplitude during a stepwise test executed at 1 Hz and load ratio of 0.1. Fatigue limit is calculated as the intersection of the two straight lines interpolating experimental thermographic data for stresses below and above the fatigue limit as explained by Luong [21]and Curà et al. [22].

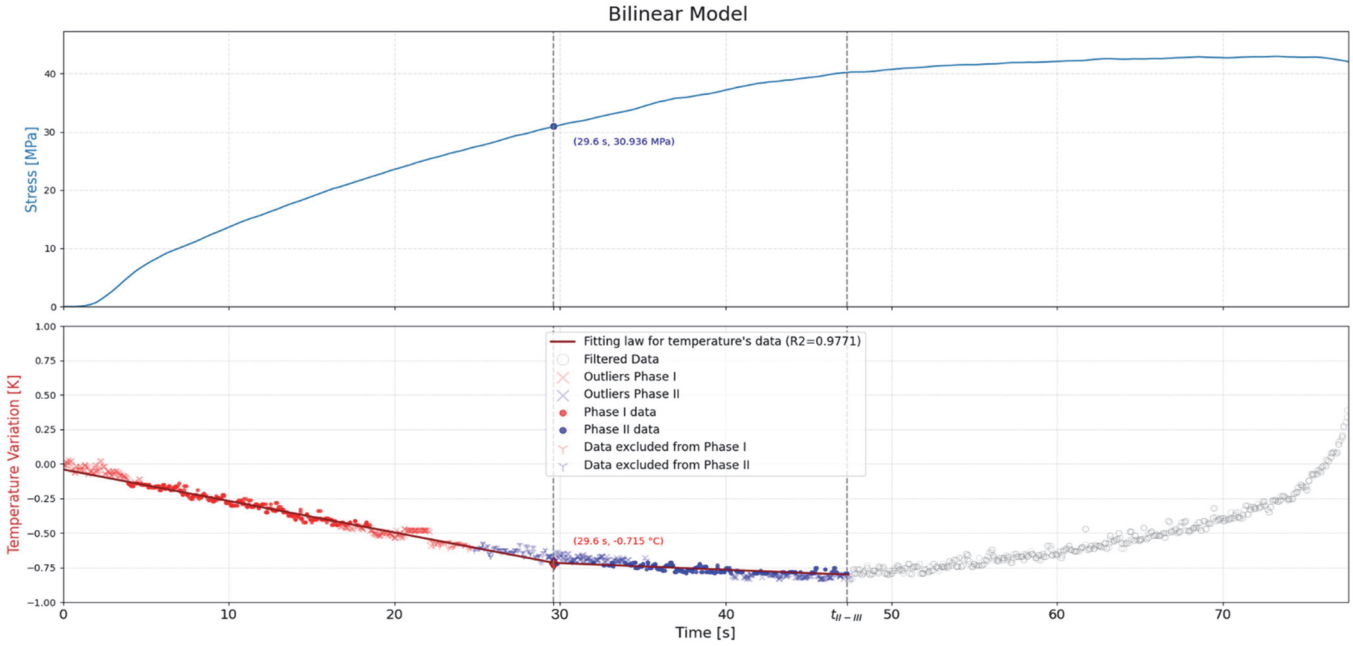

Figure 10: Static Thermographic Method's result for PA12-MJF.

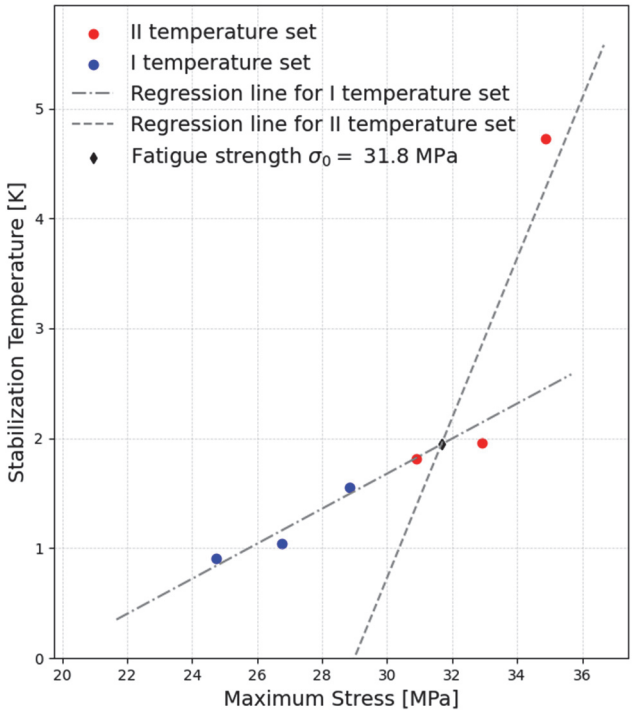

Figure 11: Risitano's Thermographic Method's result for PA12-MJF.

Both methods yield approximately the same results, as shown in Tab. 1, where the percentage errors between the STM and RTM results are 2.6%, 5.1%, and 0.06% for Nylon CF, PA12 MJF, and AISI316L, respectively, suggesting that limit stress obtained by STM can be adopted for design purposes in fatigue applications.
In Tab. 2 average values of fatigue limits and limit stresses for different materials are reported together with one standard deviation calculated as reported in ASTM D638 standard. The limit stress, σ_{lim}, predicted is the one estimated by operator and the one calculated is the one obtained by the algorithm described before.

Material	σ_{lim} [MPa] STM - Predicted	σ_{lim} [MPa] STM - Calculated	σ_0 [MPa] (RTM)	E%
Nylon CF [23]	26.8±1.2	30.1±1.3	30.9±0.1	2.6
PA12 (MJF) [7]	29.2±1.0	30.3±1.4	31.8 [7]	5.1
AISI 316L [24]	204±8	219.4±24.2	219.3±9.5	0.06

Table 2: Comparison between STM and RTM.

Stepwise fatigue tests and STM results for PA12 MJF were compared to literature's data reported in [18]. Comparison between fatigue tests executed at different load ratios is possible if S-N curves are expressed in terms of maximum stress and not in terms of stress amplitude [25] It has been observed that Thermographic Methods gave results similar to those obtained with constant amplitude tests net of the dispersion of the mechanical properties typical of this material [26]. Avanzini et al. estimated fatigue limit in correspondence of 10^6 cycles equal to 27.7 MPa, while by using fitting coefficient reported by Rosso et al. [27] it is possible to calculate a fatigue limit of 30.16 MPa. In Fig. 12 it is represented how first limit stress determined by STM and fatigue limit calculated by RTM are in Avanzini's confidence interval.

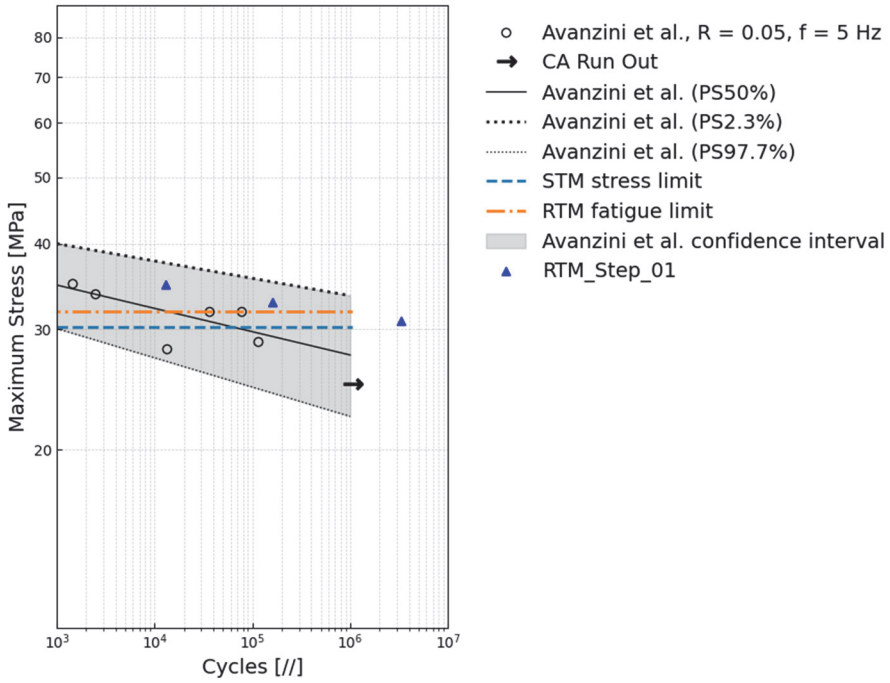

Figure 12: STM and RTM results vs. literature's SN curve

AISI 316L results obtained by RTM and STM were compared to the one reported by Werner et al. [28] In which the fatigue limit is estimated to fall within the range of 210–220 MPa based on the observed runouts and failures.

Conclusion

An objective and user-friendly method to obtain limit stress using iterative algorithms has been developed. The bilinear model method is an effective algorithm which can give accurate results about the position of the inflection point between Phase I and Phase II and the stress measured when this phenomenon occurs. The optimization of the coefficient of determination for the bilinear model, the product of the coefficient of determination of the two regression lines and the coefficient of determination of the single line for the entire dataset confirm what is found with the operator-aided method. Since a critical judgment by the operator is essential, the interactive approach to selecting separation points between phases remains a crucial tool that should not be overlooked. Algorithm was applied to quasi-static monotonic tensile tests carried out on polymers and steels specimens; STM's analysis led to the determination of the stress limit for Nylon CF, PA12 MJF and AISI316L, resulting respectively in 30.1±1.3 MPa, 30.18±1.4 MPa and 219.4±24.2 MPa. Comparison with RTM results obtained for the same materials resulted in percentage differences of 2.6%, 5.1% and 0.06%. Traditional fatigue testing campaign reported in literature showed how TM's results fall inside the dispersion band characterizing SN curve and fatigue limit determined through CA fatigue tests and staircase.

Given that the phenomenon of interest occurs within the elastic region of the stress–strain curve, the algorithm proposed is expected to remain valid without major adjustments for brittle materials. However, materials such as brittle steels, alloys and polymers, composites with multiple damage mechanisms, or specimens tested at high temperatures may present additional challenges, such as reduced signal duration, noisier signals or overlapping thermal events.

Future algorithm developments could focus on implementing machine learning-based classification to better distinguish between multiple thermal events or to distinguish material contribution to temperature variations during high temperatures tests.

Finally, the simplicity of bilinear model resulted to be enough to spot inflection point, but it is not suitable for accurately describing the entire thermal trend. For this reason, next works will focus on finding a more adequate fitting model by using machine learning algorithms and on enhancing the current algorithm by implementing advanced unsupervised learning techniques, particularly clustering and segmentation methods, to improve the detection of transition points in thermal signals. Techniques such as K-means, Gaussian Mixture Models (GMM), or density-based clustering algorithms (e.g.,

DBSCAN) may allow for more accurate and automated identification of regime changes without requiring prior assumptions on the data distribution.
In addition to unsupervised techniques, future developments may also explore supervised machine learning algorithms to further refine transition detection. For this purpose, a labelled dataset will be required. A possible strategy is to use the current algorithm to automatically generate reliable training labels for the identification of thermal phases.

REFERENCES

[1] La Rosa, G., Risitano, A. (2000). Thermographic methodology for rapid determination of the fatigue limit of materials and mechanical components, Int J Fatigue, 22, pp. 65–73. DOI: https://doi.org/10.1016/S0142-1123(99)00088-2.
[2] Fargione, G., Geraci, A., La Rosa, G., Risitano, A. (2002). Rapid determination of the fatigue curve by the thermographic method, Int J Fatigue, 24, pp. 11–19. DOI: https://doi.org/10.1016/S0142-1123(01)00107-4.
[3] Lipski, A. (2016). Accelerated determination of fatigue limit and SN curve by means of thermographic method for X5CrNi18-10 steel, Acta Mechanica et Automatica, 10, pp. 22–27. DOI: https://doi.org/10.1515/ama-2016-0004
[4] Lipski, A. (2016). Rapid Determination of the S-N Curve for Steel by means of the Thermographic Method, Advances in Materials Science and Engineering, 2016, pp. 1–7. DOI: https://doi.org/10.1155/2016/4134021.
[5] Palumbo, D., Galietti, U. (2014). Characterisation of steel welded joints by infrared thermographic methods, Quant Infrared Thermogr J, 11, pp. 29–42. DOI: https://doi.org/10.1080/17686733.2013.874220
[6] Prochazka, R., Dzugan, J., Konopik, P. (2017). Fatigue limit evaluation of structure materials based on thermographic analysis, Procedia Structural Integrity, 7, pp. 315–320. DOI: https://doi.org/10.1016/j.prostr.2017.11.094.
[7] D'Andrea, D., Crisafulli, D., Risitano, G., Santonocito, D. (2025). Thermography based approach for the rapid assessment of damage in PA12 obtained by Multijet-Fusion printing technology, Procedia Structural Integrity, pp. 449–458. DOI: https://doi.org/10.1016/j.prostr.2024.11.097.
[8] Vergani, L., Colombo, C., Libonati, F. (2014). A review of thermographic techniques for damage investigation in composites, Fract. Struct. Integr. Ann, 8. DOI: https://doi.org/10.3221/IGF-ESIS.27.01
[9] Montesano, J., Fawaz, Z., Bougherara, H. (2013). Use of infrared thermography to investigate the fatigue behavior of a carbon fiber reinforced polymer composite, Compos Struct, 97, pp. 76–83.
DOI: https://doi.org/10.1016/j.compstruct.2012.09.046.
[10] Risitano, A., Risitano, G. (2013). Determining fatigue limits with thermal analysis of static traction tests, Fatigue Fract Eng Mater Struct, 36, pp. 631–639. DOI: https://doi.org/10.1111/ffe.12030.
[11] Colombo, C., Salerno, A., Teyssiéras, A., Biffi, C.A. (2025). Rapid Assessment of Ti-6Al-4V Fatigue Limit via Infrared Thermography, Metals, 15(8), 825. DOI: https://doi.org/10.3390/met15080825.
[12] Crisafulli, D., Foti, P., Berto, F., Risitano, G., Santonocito, D. (2025). An innovative and sustainable methodology for fatigue characterization and design, Eng Fract Mech, 315, 110854.
DOI: https://doi.org/10.1016/J.ENGFRACMECH.2025.110854.
[13] Williams, P., Liakat, M., Khonsari, M.M., Kabir, O.M. (2013). A thermographic method for remaining fatigue life prediction of welded joints, Mater Des, 51, pp. 916–923. DOI: https://doi.org/10.1016/j.matdes.2013.04.094
[14] Curà, F., Gallinatti, A.E., Sesana, R. (2012). Dissipative aspects in thermographic methods, Fatigue Fract Eng Mater Struct, 35, pp. 1133–1147. DOI: https://doi.org/10.1111/j.1460-2695.2012.01701.x.
[15] Melvin, A.D., Lucia, A.C., Solomos, G.P., Volta, G., Emmony, D. (1990). Thermal emission measurements from creep damaged specimens of AISI 316L and Alloy 800H, in: Proc 9th Int Conf Exp Mech, pp. 765–773.
[16] Corigliano, P., Cucinotta, F., Guglielmino, E., Risitano, G., Santonocito, D. (2020). Fatigue assessment of a marine structural steel and comparison with Thermographic Method and Static Thermographic Method, Fatigue Fract Eng Mater Struct, 43, pp. 734–743. DOI: https://doi.org/10.1111/ffe.13158.
[17] Rodríguez-Reyna, S.L., Mata, C., Díaz-Aguilera, J.H., Acevedo-Parra, H.R., Tapia, F. (2022). Mechanical properties optimization for PLA, ABS and Nylon + CF manufactured by 3D FDM printing, Mater Today Commun, 33, 104774.
DOI: https://doi.org/10.1016/j.mtcomm.2022.104774.
[18] Avanzini, A., Battini, D., Pandini, S. (2022). Static and fatigue behavior in presence of notches for polyamide 12 (PA12) additively manufactured via Multi Jet FusionTM process, Int J Fatigue, 161, 106912.
DOI: https://doi.org/10.1016/j.ijfatigue.2022.106912.
[19] Riaz, M. (2015). On Enhanced Interquartile Range Charting for Process Dispersion, Qual Reliab Eng Int, 31, pp. 389–398. DOI: https://doi.org/10.1002/qre.1598.

[20] Zaeimi, M., De Finis, R., Palumbo, D., Galietti, U. (2024). Fatigue limit estimation of metals based on the thermographic methods: A comprehensive review, Fatigue Fract Eng Mater Struct, 47, pp. 611–646. DOI: https://doi.org/10.1111/ffe.14206.
[21] Luong, M.P. (1995). Infrared thermographic scanning of fatigue in metals, Nuclear Engineering and Design, 158, pp. 363–376. DOI: https://doi.org/10.1016/0029-5493(95)01043-H.
[22] Curà, F., Curti, G., Sesana, R. (2005). A new iteration method for the thermographic determination of fatigue limit in steels, Int J Fatigue, 27, pp. 453–459. DOI: https://doi.org/10.1016/j.ijfatigue.2003.12.009.
[23] D'Andrea, D., Risitano, G., Corigliano, P., Santonocito, D., D'Andrea, D. (2025). Mechanical characterization of Nylon CF printed by FDM process by using energy methods, Procedia Structural Integrity, 68, pp. 746–755. DOI: https://doi.org/10.1016/J.PROSTR.2025.06.125.
[24] D'Andrea, D., Risitano, G., Corigliano, P., D'Andrea, D. (2025). Fatigue Strength Determination of AISI 316L Steel and Welded Specimens Using Energy Methods, in: AIAS 2024, MDPI, Basel Switzerland, p. 31. DOI: https://doi.org/10.3390/engproc2025085031.
[25] Ezeh, O.H., Susmel, L. (2019). Fatigue strength of additively manufactured polylactide (PLA): effect of raster angle and non-zero mean stresses, Int J Fatigue, 126, pp. 319–326. DOI: https://doi.org/10.1016/J.IJFATIGUE.2019.05.014.
[26] Khorasani, M., MacDonald, E., Downing, D., Ghasemi, A., Leary, M., Dash, J., Sharabian, E., Almalki, A., Brandt, M., Bateman, S. (2024). Multi Jet Fusion (MJF) of polymeric components: A review of process, properties and opportunities, Addit Manuf, 91, 104331. DOI: https://doi.org/10.1016/J.ADDMA.2024.104331.
[27] Rosso, S., Meneghello, R., Biasetto, L., Grigolato, L., Concheri, G., Savio, G. (2020). In-depth comparison of polyamide 12 parts manufactured by Multi Jet Fusion and Selective Laser Sintering, Addit Manuf, 36, 101713. DOI: https://doi.org/10.1016/J.ADDMA.2020.101713.
[28] Werner, T., Madia, M., Zerbst, U. (2022). Comparison of the fatigue behavior of wrought and additively manufactured AISI 316L, Procedia Structural Integrity, 38, pp. 554–563. DOI: https://doi.org/10.1016/J.PROSTR.2022.03.056.

NOMENCLATURE

B	Burgess vector
c	Specific heat
CA	Constant amplitude fatigue test
$CI_{95\%}$	95% Confidence Interval
DIC	Digital Image Correlation
E	Young's Modulus
FFM	Fast Fatigue Machine
IQR	Interquartile Range
K_m	Thermoelastic constant
m_1	First regression line's slope
m_2	Second regression line's slope
n	Number of observations
N_i	Cycles
q_1	First regression line's intercept
q_2	Second regression line's intercept
R_1^2	First regression line's determination coefficient
R_2^2	Second regression line's determination coefficient
R_{bl}^2	Bilinear model's determination coefficient
R_{sl}^2	Single line parameter
RTM	Risitano's Thermographic Method
s	Standard deviation
STM	Static Thermographic Method
t^*	Student's t

$t_{II,III}$	Separation's instant between phase II and phase III
t_{int}	Intersection between regression lines instant
T_0	Specimen initial surface temperature
TM	Thermographic Method
α	Coefficient of thermal expansion
ϕ	Energy Parameter
ΔT	Temperature's variation
$\overline{\Delta T}$	Temperature's variation's mean value
ΔT_{bl}	Temperature's variation calculated by bilinear model
$\Delta T_{fit,\ I}$	Temperature variation calculated with the first regression line
$\Delta T_{fit,\ II}$	Temperature variation calculated with the second regression line
ΔT_I	I phase's temperature's variation
$\overline{\Delta T_I}$	I phase's temperature variations mean value
$\Delta T_{I,II}$	Temperature's variation corresponding to first damage arise
ΔT_{II}	II phase's temperature's variation
$\overline{\Delta T_{II}}$	II phase's temperature variations mean value
ΔT_s	Surface temperature's variation
ΔT_{sl}	Temperature's variation calculated with single regression line
ΔT_{st}	Stabilization temperature
ΔT_{int}	Temperature's variation calculated as the intersection between first and second regression lines
ρ	density
$\sigma_{0,RTM}$	Fatigue limit calculated by RTM
σ_1	First principal stress
$\sigma_{lim,STM}$	Limit stress calculated by STM